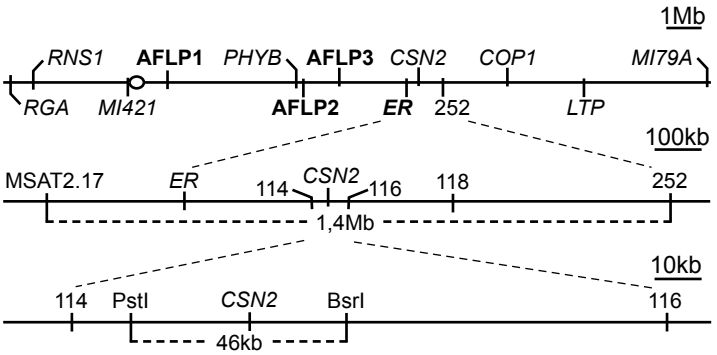

Supplemental Figure 1: Map-based isolation of the *csn2-5* mutation.

Chromosome landing at the *csn2-5* locus was initiated by a combination of bulk-segregant/ AFLP analysis. AFLP markers are shown in bold. A window containing *csn2-5* was defined and refined using micro-satellite and (d)CAPS markers. Corresponding portions of chromosome 2 are shown with their respective scales. A 46-kb window encompassing *csn2-5* was defined.

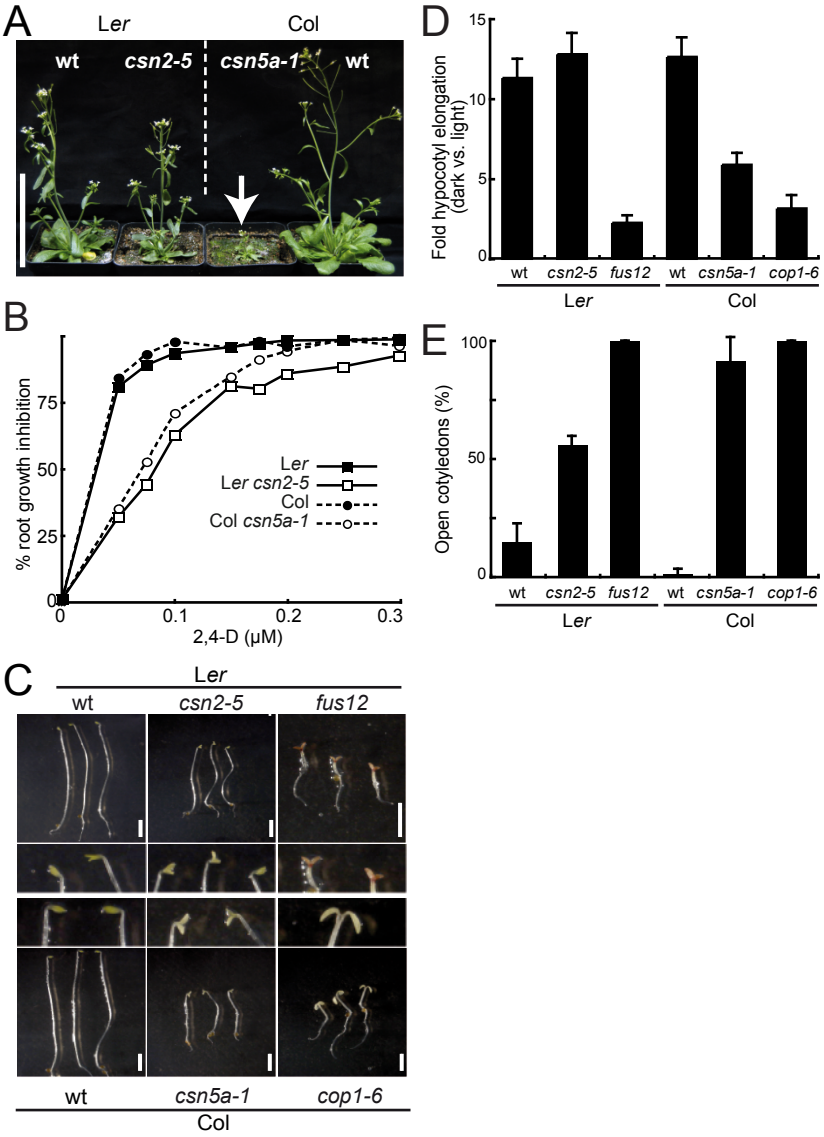

Supplemental Figure 2: Relative physiological and molecular characterization of the *csn2-5* and *csn5a-1* mutants

(A) Morphology of five-weeks-old plants grown under long day conditions. Scale = 10 cm. (B) Inhibition of root elongation by increasing concentrations of synthetic auxin 2,4-D. Data points are averages of 8 seedlings and standard deviations were less than 10%. Measurements of root elongation were performed on 8-days-old seedlings, 3 days after transfer on auxin-containing medium. One representative experiment out of three repetitions is shown. (C, D, E) Arabidopsis plants were incubated for 6 h under light conditions to induce germination and returned to complete darkness for 4 d. Photographs were taken immediately and used for scoring cotyledon opening (n≥20) (E) and hypocotyls elongation(n≥20) (D). Error bars represent standard deviations. One representative experiment out of three is shown. wt: wild type.

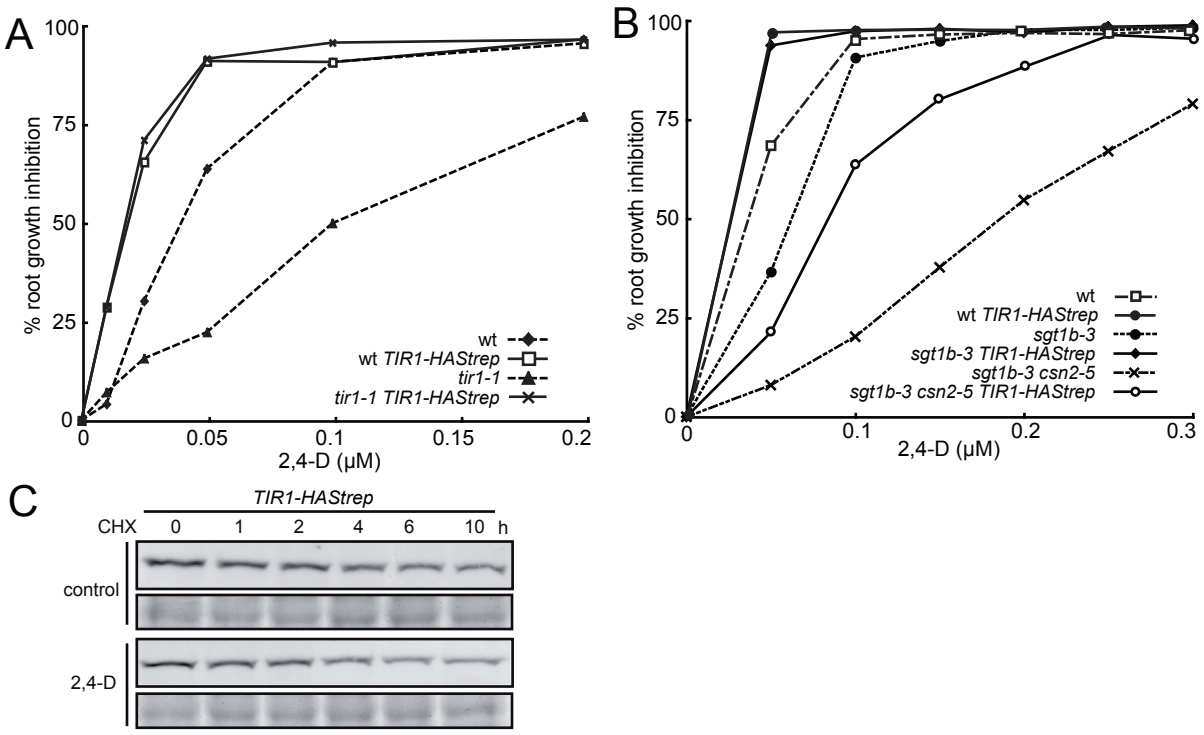

Supplemental Figure 3: Physiological and biochemical characterization of *TIR1-HAStrep* transgenic plants

(A) Complementation of the *tir1-1* mutation by *TIR1-HAStrep* expressed from its own promoter was tested in the root growth inhibition assay with increasing concentrations of 2,4-D. *TIR1-HAStrep* transgene was initially transformed into Col-0 *tir1-1* and subsequently crossed to Col-0 to generate Col-0 *TIR1-HAStrep*. Data points are the average of at least 10 seedlings. One representative experiment out of three is shown. Standard deviations were <10%.

(B) Inhibition of root elongation by increasing concentrations of 2,4-D. *TIR1-HAStrep* transgene was initially transformed into L*er* and sequentially introgressed into L*er sgt1b-3* and L*er sgt1b-3/csn2-5*. Data points are the average of at least 10 seedlings. Standard deviations were <10%, one representative experiment out of three is shown. Standard deviations were <10%.

(C) TIR1-HAStrep is not a short-lived F-box protein. Cycloheximide (CHX, 100µM) was used to block translation and evaluate stability of TIR1-HAStrep in the wild-type Ler genotype with and without addition of auxin (5µM 2,4-D). Seedlings were harvested at the indicated time points after addition of CHX and total protein extracts analyzed on immunoblots with anti-HA antibody. A coomassie-stained portion of the gel is shown to evaluate relative loading of the samples.

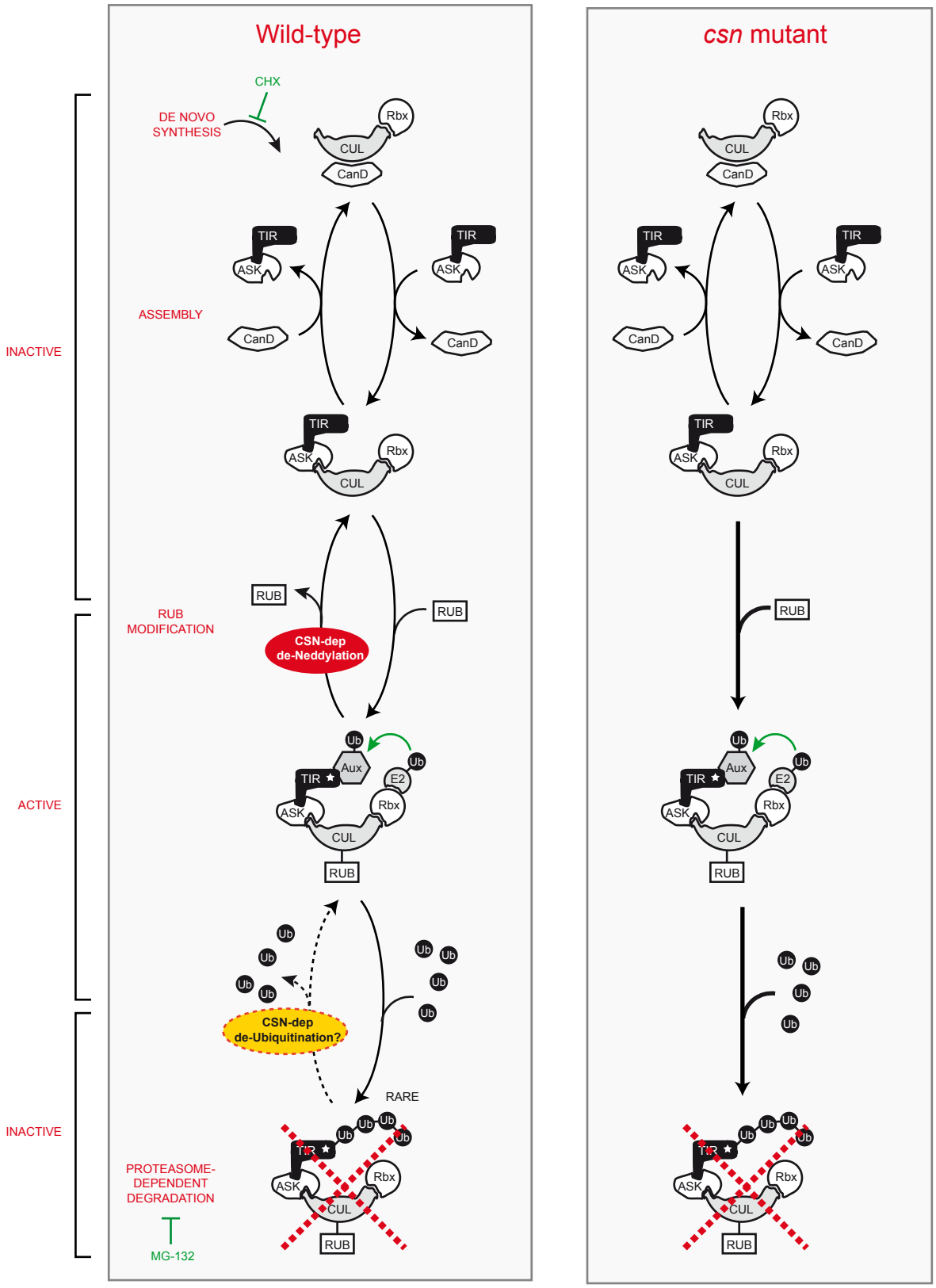

Supplemental Figure 4: Model for post-translational regulation of SCF^{TIR1} activity in wild-type and *csn* mutants

Disassembly of CAND1 from CUL1 allows neddylation of CUL1 and assembly of an active SCF^{TIR1} auxin receptor. Upon auxin binding, Aux/IAA proteins are poly-ubiquitinated and ultimately targeted for proteasome-dependent degradation. SCF^{TIR1} can be inactivated by CSN-mediated deneddylation and individual SCF components are recycled. As a rare event, TIR1 ubiquitination causes SCF^{TIR1} inactivation and degradation thus diminishing auxin perception and downstream responses. In *csn* mutants, SCF^{TIR1} components cannot be recycled and are sent preferentially for degradation by the ubiquitin/proteasome pathway thus explaining the auxin insensitive phenotype of those mutants. Ub, ubiquitin; CUL, cullin; ASK, Arabidopsis SKP1; TIR, TIR1; Aux, AUX/IAA; RUB, NEDD8/RUB modification; CanD, CanD1; CSN, COP9 signalosome; white asterix, auxin.

Stuttmann et al